Eur. Phys. J. B **46**, 251–255 (2005)
DOI: 10.1140/epjb/e2005-00248-6

THE EUROPEAN PHYSICAL JOURNAL B

Synchrotron X-ray diffraction study of $SrRuO_3/SrTiO_3/SrRuO_3$ nano-sized heterostructures grown by laser MBE

C. Aruta[1,a], M. Angeloni[1], G. Balestrino[1], P.G. Medaglia[1], P. Orgiani[1], A. Tebano[1], and J. Zegenhagen[2]

[1] Coherentia CNR-INFM and Dipartimento di Ingegneria Meccanica, Università di Roma "TorVergata", via del Politecnico 1, 00133 Roma, Italy
[2] ESRF, European Synchrotron Radiation Facility, B.P. 220, 38043 Grenoble Cedex, France

Received 10 January 2005 / Received in final form 30 May 2005
Published online 11 August 2005 –

Abstract. Structural investigation using X-ray synchrotron radiation has been performed on $SrRuO_3/SrTiO_3/SrRuO_3$ epitaxial heterostructures, with each constituent layer a few unit cell thick grown on (001) $SrTiO_3$ substrate. Detailed information on the evolution of the in-plane lattice structure has been obtained, in these heterostructures, by grazing incidence diffraction measurements. The samples have been grown by low-pressure pulsed laser deposition. Under our deposition conditions, $SrRuO_3$ layers grow with an elongated cell perpendicular to the substrate surface. The in-plane pseudocubic lattice parameters do not match the in-plane square $SrTiO_3$ structure even in the case of very thin $SrRuO_3$ layers. Such a distortion was found to decrease with increasing the thickness of the $SrTiO_3$ barrier layer.

PACS. 81.15.Fg Laser deposition – 61.10.Nz X-ray diffraction – 68.55.Ac Nucleation and growth: microscopic aspects

1 Introduction

Heterostructures based on perovskite oxides can be relevant for device applications, due to the broad range of technologically important properties (ranging from insulating to metallic and from paramagnetic to ferromagnetic) and the structural and chemical similarities of such materials [1–3]. It is well known that the strain and lattice distortions or even the film thickness can strongly affect the electrical and magnetic properties of perovskite oxide films, such as the manganite- [4] and ruthenate- [5] based films. In the case of heterostructures, these effects are even more pronounced due to the larger number of interfaces. However, the choice of the relative thickness of the constituent layers in an heterostructure is motivated by the targeted device performances. Therefore, for the fabrication of specific heterostructures, the influence of the relative layer thickness on the crystallographic structure must be understood in detail. In this paper, we report a structural investigation by synchrotron radiation of $SrRuO_3/SrTiO_3/SrRuO_3$ trilayers. Because of their interesting physical properties and structural similarity, $SrRuO_3$ and $SrTiO_3$ are very important building blocks for designing heterostructures for device applications. Strontium ruthenate $SrRuO_3$ (SRO) is a conducting ferromagnet with a Curie temperature of ∼150–160 K [6]. Because of its high chemical and thermal stability SRO has attracted considerable interest as an electrode [7] or barrier layer [8]. Strontium titanate $SrTiO_3$ (STO), owing to its electric field dependence of the dielectric constant, is a very attractive material for microwave applications [9]. Some papers have been published on the stress relaxation mechanism of SRO/STO bilayers [10,11], composed by thick constituent layers (from tens to thousands of nanometers). In this study we investigate the structural properties of SRO/STO/SRO trilayers which are composed of very thin blocks (a few unit cells). Most of devices are based on the trilayer structure. However a different propagation of the strain field along the whole structure, can give rise to a different stress experienced by each constituent layer in the trilayers respect to the bilayers. Indeed, in the case of a partial relaxation of the first SRO layer, the thin STO intermediate layer can be itself strained, thus influencing the growth of the second SRO layer in a different manner respect to the first SRO layer deposited on the STO substrate. Therefore, SRO/STO/SRO trilayers represent a useful model to understand the variation of the structural properties when perovskite oxide layers are stacked on top of each other to form nano-sized heterostructures for device applications.

At room temperature bulk SRO exhibits the $GdFeO_3$ orthorhombic structure [12], but it can be indexed as a pseudo-cubic perovskite with a lattice constant of

[a] e-mail: carmela.aruta@uniroma2.it

$a = 3.930$ Å. The degree of the orthorhombic distortion decreases with increasing temperature, and the structure transforms to tetragonal at 547 °C and to the standard cubic perovskite structure at 677 °C [13]. Bulk STO has a simple cubic perovskite structure, at room temperature, with a lattice constant $a_{\mathrm{STO}} = 3.905$ Å. It undergoes a cubic to tetragonal antiferrodistortive transition at about 378 °C.

When SRO films are deposited on (001) STO substrate, they can grow epitaxially with two different growth directions: with the orthorhombic [001] or the [110] axis normal to the (001)STO surface. Several articles [14–16] reported the growth along the orthorhombic [110] direction with the presence of 90° domains in the plane. However, the results reported in references [14] and [16] indicate that the misorientation of the substrate induces the growth of single domain films. It has also been reported [17] that SRO thin films, on stepped STO substrate, grow with the prototypical cubic perovskite structure. At the end of the deposition process, the transition to orthorhombic symmetry upon cooling involves a tilting of the oxygen octahedral and an angular distortion of the unit cell which results in a pseudo monoclinic perovskite subcell. Due to the relatively small mismatch between SRO and STO lattice parameters, it is possible to obtain epitaxial SRO/STO/SRO heterostructures [18]. In this paper we investigate the influence of the relative thickness of the STO and SRO layers on the in-plane distortions in such heterostructures, by grazing incidence diffraction measurements with synchrotron radiation. Different SRO/STO/SRO heterostructures were investigated keeping the total thickness constant but varying the number of unit cells of the STO and SRO layers. The thickness of all SRO layers is well below the threshold value for the occurring of the ferromagnetic transition [5].

2 Experimental details

SRO/STO/SRO heterostructures were grown by pulsed laser deposition with the in-situ reflection high energy electron diffraction diagnostic (RHEED). The growth was performed with about 3 J/cm^2 energy density of excimer pulsed laser source. The target-to-substrate separation distance was 10 cm and growth pressure was in the 10^{-4} Pa range, obtained with a mixture of molecular oxygen and 10% ozone. The samples were deposited on (001) STO single crystal substrates. Prior to deposition, the substrates were chemically etched following the procedure of Kawasaki et al. [19], and subsequently degassed in oxygen atmosphere [20]. This process reduced the step density on the surface as demonstrated by RHEED specular spot intensity. The miscut of the substrate was experimentally determined and the angle between the surface normal and the crystallographic [001] direction was found to be about 0.25° (see below). By monitoring the RHEED intensity oscillations, a precise control on the thickness of each layer of the heterostructure was possible. We obtained heterostructures with an error on the thickness of each individual layer much smaller than a single unit cell and a low interface roughness, as confirmed by specular X-ray reflectivity measurements [18]. Further details on the deposition process and the transport properties of SRO films are reported elsewhere [5].

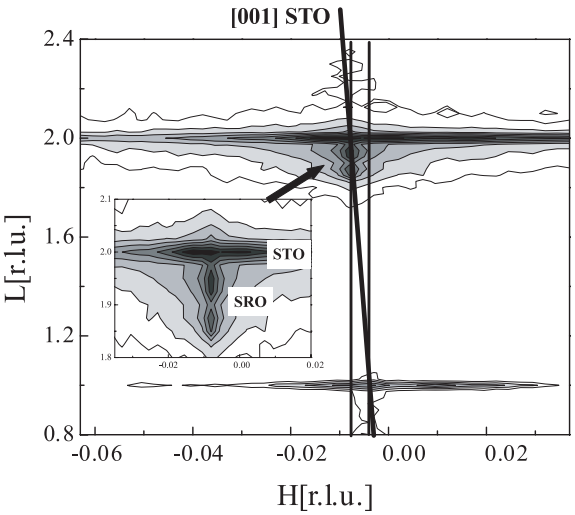

Fig. 1. Isointensity contour plot in logarithmic scale of $H - L$ map around the (021) and (022) reflections of the 11/5/11 heterostructure.

X-ray diffraction measurements were carried out at the European Synchrotron Radiation Facility in Grenoble (France) at the ID32 insertion device beamline with 16 KeV X-ray radiation. Structural characterization was performed by grazing incidence X-ray diffraction (GID) at an incidence angle of the X-rays with the sample surface of 0.2°. At this angle of incidence, the attenuation length of 16 keV X-rays was around 200 nm inside our samples. Therefore, with this measurement configuration, the scattering from the substrate was extremely reduced. We investigated $\mathrm{SRO}_M/\mathrm{STO}_N/\mathrm{SRO}_M$ heterostructures with $N + 2M = 27$ unit cells (u.c.) and with the number N of STO barrier layer from zero to 13 u.c. The measurements were performed by recording reciprocal space maps (RSM) around several reciprocal lattice points. In the following, the measurement units of the RSM are given normalized to the STO substrate lattice parameters and are denoted as reciprocal lattice units (r.l.u.). The coordinate system is defined by the cubic unit cell of the crystalline STO substrate.

3 Results and discussion

In order to obtain information on the perpendicular structural properties of the film, $H - L$ maps with a fixed value of K were performed. In Figure 1, the isointensity $H - L$ contour map around the 02L rod of the substrate is shown for the sample with $N = 5$ u.c. of STO barrier layer. Two intense peaks associated with the substrate at $L = 1$ and $L = 2$ r.l.u. are evident in the map. Two vertical straight lines are drawn along the L-direction, i.e, the direction of the diffuse scattering from the sample surface, through the (021) and (022) reflections of the film. The two lines do not coincide and their distance ΔH is proportional to the miscut angle of the substrate. The value of the miscut angle is

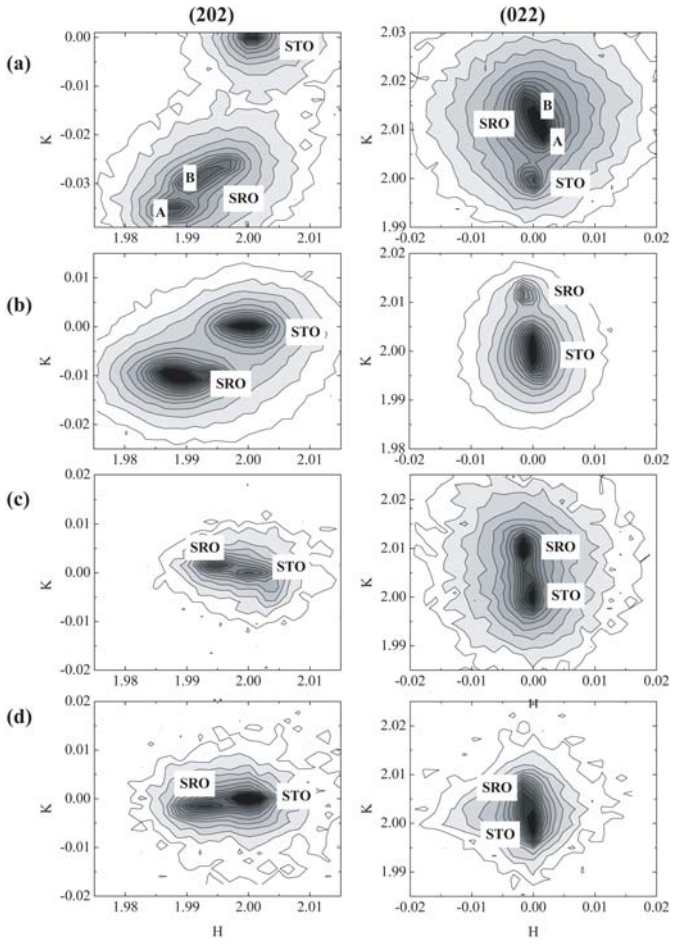

Fig. 2. Isointensity contour plots on a logarithmic scale of the (202) and (022) RSMs in $H-K$ r.l.u. of SRO/STO/SRO heretostructures. The four samples are grown on STO substrates and (a) refers to the SRO film (0 u.c. of STO as barrier layer), while (b), (c) and (d) refer to the 11/5/11, 9/9/9 and 7/13/7 heterostructures respectively. All the r.l.u. intervals are 0.04 large.

obtained by $\tan^{-1}(\Delta H/\Delta L)$ and in this case results to be $0.25 \pm 0.01°$. For $L < 2$ it is possible to distinguish, in the map, the presence of the intensity oscillations related to SRO(022). The oscillations are caused by the splitting of the SRO peak due to the interference effects generated by the intermediate STO layer in the sandwiched heterostructure. It is difficult to identify the same effect on the (021) reflection due to the smaller separation between the SRO and STO reflections. This interference effect was already shown in the specular diffraction measurements performed on the same samples, as reported in reference [18], and it is also an indication of sharp and well-defined interfaces.

In-plane structural properties were investigated by $H-K$ mapping around several reciprocal lattice points. In Figure 2 the results obtained for the (202) and (022) reflections are reported in the case of samples with 0, 5, 9, 13 u.c. of STO barrier layer. (202) and (022) reflections allow to determine the a and b lattice parameters separately and the in-plane relationship between the film and the substrate. In all the RSMs of Figure 2 the SRO reflections close to the (202) and (022) STO reflections can be distinguished.

Table 1. Lattice parameters of the SRO perovskite subunit cell in $SRO_M/STO_N/SRO_M$ heterostructures. The in-plane a and b lattice parameters are the longer and the shorter axes respectively, obtained by GID measurements. The c-axis parameter were previously obtained by specular diffraction measurements [18].

Sample ($M/N/M$ u.c.)	a(Å) ±0.002	b(Å) ±0.002	c(Å) ±0.002
27/-/- *(domain A)*	3.928	3.886	4.094
27/-/- *(domain B)*	3.921	3.881	
11/5/11	3.927	3.883	4.094
9/9/9	3.915	3.886	4.041
7/13/7	3.917	3.898	4.041

In the case of no STO barrier layer (maps in Fig. 2a), two different peaks for SRO can be distinguished. They are labeled as A and B in Figure 2a. The two peaks *cannot* be associated with the typical twin domains, i.e., the two possible orientations of the rectangular unit cell of the orthorhombic SRO on the square unit cell of the cubic STO, because they are not symmetric relative a 90 degrees rotation in the reciprocal lattice space. We have indicated with A and B the stronger and weaker peaks respectively, in both STO(202) and (022) maps of Figure 2a. Therefore, we associate one domain to the couple of A-peaks and the other domain to the couple of B-peaks. However, in the case of 5, 9 and 13 u.c. of STO barrier layers (Figs. 2b–d), only one domain can be distinguished in the maps. Differing with many reports [14–16], we have not observed any twin-domains in our samples. This finding can be explained by the misorientation angle of the substrate which is sufficient to destroy the fourfold symmetry of the (001) STO surface. Since no extra peaks are observed in the maps, the STO intermediate layer must assume either the SRO or most likely the STO bulk lattice constant. The in-plane a and b lattice parameters (reported in Tab. 1) can be obtained from the (202) and (022) RSMs of Figure 2 by a_{STO} H_{STO}/H_{SRO} and a_{STO} K_{STO}/K_{SRO} respectively, showing that that a and b are the longer and the shorter in-plane axes, respectively.

The c-axis parameters of the perovskite subunit cell reported in the same table were previously calculated by simulation of the diffraction measurements in specular configuration around the (002) reflection [18]. For SRO thin films and SRO/STO/SRO heterostructures, grown under our deposition conditions, the values of the c lattice parameters are very large and cannot be explained by simply applying elasticity theory, because it would result in a too large Poisson coefficient. Nevertheless, in the case of 600 Å thick SRO films, grown with the same deposition conditions, the c lattice parameter resulted to be 3.96 Å [5]. This value is already larger compared to the pseudocubic bulk value of 3.93 Å commonly quoted for polycrystalline and single crystal SRO samples. This effect, noticed also in thicker SRO films, could be ascribed to ion bombardment during the growth process [21].

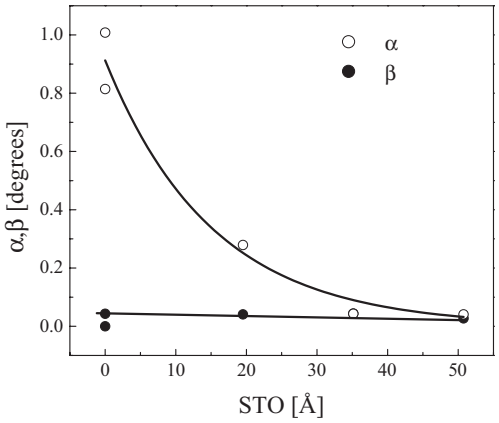

Fig. 3. Behavior of the angles α and β between the in-plane SRO axes and the [100] and the [010] STO directions respectively, as a function of the number of STO u.c. of the barrier layer.

Furthermore, for manganites compounds, structurally very similar to SRO, it had been shown that the c-axis lattice parameter of thin films increases in the case of growth by PLD in low oxygen pressure environment [22,23].

In the RSMs of Figure 2 it can be also seen that the in-plane crystallographic directions of the SRO layers, indexed in the pseudocubic notation, are not perfectly parallel to the unit cell axes of STO substrate. From the peak positions we can calculate the angles α and β which the in-plane directions form with the [100] and [010] STO in-plane directions respectively, by $\alpha = \tan^{-1}(K/H)$ and $\beta = \tan^{-1}(H/K)$, where (H, K) are the Miller indices for the SRO reflections. The absolute values of the angles calculated from the maps are reported in Figure 3 as a function of the number of unit cells of STO barrier layer.

The larger angle α is the angle that the a-axis (the longer axis) forms with the [100] crystallographic direction of STO and the lower angle β is the angle that the b-axis (the shorter axis) forms with the [010] direction. Therefore, it is the longer axis which rotates the most in order to accommodate the mismatched STO square cell. From the behaviour of the angles of rotations as a function of the number of STO unit cells (Fig. 3), it can be observed that the smaller angle β, which is close to zero anyway, remains almost constant while the higher angle α decreases drastically on increase in the number of the unit cells of the STO barrier layer. The in-plane lattice parameters (Tab. 1) accordingly become more and more similar to those of STO. The dependence of the SRO lattice distortion and parameters on the relative thickness of SRO and STO, is a clear indication of the effect of the epitaxial strain in the SRO/STO/SRO heterostructures grown on (001) STO substrate.

4 Conclusions

It is well known that the deposition conditions as well as the films thickness significantly affect the films intrinsic properties and the interface characteristics in the heterostructures. This aspect becomes particularly relevant for potential devices, since structural distortions at the interfaces can dramatically influence the tunneling properties across different layers. In this respect, a detailed investigation of the structural properties of very thin layers in the heterostructures becomes fundamental. We have performed a GID investigation of SRO/STO/SRO heterostructures and we have found that, by PLD in low background oxygen pressure, even the very first SRO layers are not pseudomorphic. In particular, SRO constituent layers grow with an elongated cell perpendicular to the STO surface. No twinning domains have been observed in SRO layers most likely because of the miscut of the substrate surface. Two different angles of rotation of the SRO axis parameters with respect to the STO in-plane crystallographic directions, have been observed. The larger angle is formed by the longer axis. Such a distortion varies as a function of the SRO layer thickness because of the strain provided by both the substrate and the STO barrier layer. By increasing the thickness of the intermediate layer and thus decreasing the thickness of the SRO layers, the distortion and the orthorhombicity of the unit cell decrease, approaching the square unit cell of the STO. In conclusion, PLD is a very versatile growth technique to obtain perovskite heterostructures with good interfaces quality. However, our results demonstrate that high structural distortions can be present at the interfaces, which strongly depend on the thickness of the constituent layers. It is fundamental a deeper investigation of the role of such distortions in the performances of new devices based on perovskite oxides with functional properties.

We would like to thank all the staff of ID32 beamline at ESRF and in particular T.L. Lee for the helpful assistance during the experiment.

References

1. See e.g.: *Colossal-magnetoresistive manganite thin films* edited by W. Prellier, Ph. Lecoeur, B. Mercey, J. Phys.: Condens. Matter **13**, R915 (2001)
2. H.Y. Hwang, S.W. Cheong, N.P. Ong, B. Batlog, Phys. Rev. Lett. **77**, 2041, (1996)
3. S. Jin, T.H. Tiefel, M. McCormack, R.A. Fastnach, R. Ramesh, L.H. Chen, Science **264**, 413 (1994)
4. R.A. Rao, D. Lavric, T.K. Nath, C.B. Eom, L. Wu, F. Tsui, Appl. Phys. Lett. **73**, 3294 (1998)
5. P. Orgiani, C. Aruta, G. Balestrino, S. Lavanga, P.G. Medaglia, A. Tebano, Eur. Phys. J. B **26**, 23 (2002)
6. P.B. Allen, H. Berger, O. Chauvet, L. Forro, T. Jalborg, A. Junod, B. Revaz, G. Santi, Phys. Rev. B **53**, 4393 (1996)
7. Q.X. Jia, X.D. Wu, S.R. Foltyn, P. Tiwari, Appl. Phys. Lett. **63**, 2570 (1993)
8. R. Domel, C.L. Jia, C. Competti, G. Ockenfuss, A.I. Branginski, Supercon. Sci. Technol. **7**, 277 (1994)
9. K. Bouzehouane, P. Woodall, B. Marcilhac, A.N. Khodan, D. Crété, E. Jacquet, J.C. Mage, J.P. Contour, Appl. Phys. Lett. **80**, 109, (2002)
10. J.S. Wu, C.L. Jia, K. Urban, J.H. Hao, X.X. Xi, J. Mater. Res. **16**, 3443, (2001)

11. Z.-G. Ban, S.P. Alpay, F. He, B.O. Wells, X.X. Xi, Appl. Phys. Lett. **84**, 4848 (2004)
12. C.W. Jones, P.D. Battle, P. Lightfoot, W.T.A. Harrison, Acta Cryst. C **45**, 365 (1989)
13. B.J. Kennedy, B.A. Hunter, Phys. Rev. B **58**, 653 (1998)
14. Q. Gan, R.A. Rao, C.B. Eom, Appl. Phys. Lett. **70**, 1962 (1997)
15. J.C. Jiang, X.Q. Pan, C.L. Chen, Appl. Phys. Lett. **72**, 909 (1998)
16. J.C. Jiang, W. Tian, X.Q. Pan, Q. Gan, C.B. Eom, Appl. Phys. Lett. **72**, 2963 (1998)
17. J.-P. Maria, H.L. McKinstry, S. Troiler-McKinstry, Appl. Phys. Lett. **76**, 3382 (2000)
18. M. Angeloni, C. Aruta, G. Balestrino, P. Orgiani, A. Tebano, P.G. Medaglia, Eur. Phys. J. B **29**, 561 (2002)
19. M. Kawasaki, K. Takahashi, T. Maeda, R. Tsuschia, M. Shinohara, O. Ishiyama, M. Yoshimoto, H. Koinuma, Science **266**, 1540 (1994)
20. G. Koster, B.L. Kropman, G.J.H.M. Rijnders, D.H.A. Blank, H. Rogalla, Appl. Phys. Lett. **73**, 2920 (1998)
21. J.-P. Maria, S. Troiler-McKinstry, D.G. Schlom, M.E. Hawley, G.W. Brown, J. Appl. Phys. **83**, 4373 (1998)
22. K.M. Krishnan, H.L. Ju, Phys. Rev. B **60**, 14793 (1999)
23. J. Dho, N.H. Hur, I.S. Kim, Y.K. Park, J. Appl. Phys. **94**, 7670 (2003)